15

High-energy electron beam induced changes in the atomic composition of materials in the TEM

© K.E. Prikhodko,[1,2] M.M. Dement'eva[1]

[1] National Research Centre „Kurchatov Institute"
123182 Moscow, Russia
[2] National Research Nuclear University „MEPhI"
115409 Moscow, Russia
e-mail: prihodko_ke@nrcki.ru

Received April 30, 2025
Revised April 30, 2025
Accepted April 30, 2025

The effect of high-energy electron irradiation (200 keV) *in situ* in a TEM (transmission electron microscope) column on samples of bismuth oxide BiO_2 polycrystalline films and copper oxide CuO films, as well as on thin samples of tantalum disulfide TaS_2 has been studied. It was found that the the electron beam exposure induce preferential displacements of light atoms from the crystal lattice nodes (for which the transferred energy E_t exceeds the threshold displacement energy E_d) in the direction of the primary electrons motion, which causes their successive removal from the sample volume and initiates the formation of phases with a reduced content of light atoms. BiO_2 samples undergo phase transformation into bismuth oxide Bi_2O_3, the first signs of which appear at fluence of $1.5 \cdot 10^{23}$ e/cm^2, and with increasing irradiation fluence up to $3.5 \cdot 10^{23}$ e/cm^2 this transformation spreads deep into the sample. At irradiation of CuO samples up to fluence $0.55 \cdot 10^{23}$ e/cm^2 copper oxide of Cu2O composition is formed, and at the fluence $3.3 \cdot 10^{23}$ e/cm^2 — metallic copper. Phase transformations in TaS_2 occur at the $1.74 \cdot 10^{23}$ e/cm^2 with the TaS formation. The model of the light atoms removal process under the action of electron irradiation has been developed. Within the framework of the developed model, the threshold displacement energy (Ed) values of oxygen atoms was found to be 31.3 eV in BiO_2, 21.5 eV in CuO, and for sulfur atoms 15.2 eV in TaS_2.

Keywords: Electron energy loss spectroscopy (EELS), high-resolution transmission electron microscopy (HRTEM), electron irradiation, electron irradiation in situ in TEM, displacement threshold energy.

DOI: 10.61011/TP.2025.10.62084.89-25

Introduction

Microstructural investigations involving transmission electron microscopy use relativistic electrons to get useful information about the structure and phase composition of test samples. However, these electrons with energies within 100−300 keV induce various types of defects in a sample, which may lead to changes both of the structure and atomic composition of materials of interest. Radiation damage induced by beam electrons is usually classified by the manner in which the damage occurs after elastic or inelastic scattering of incident electrons [1].

Elastic scattering processes include interaction between beam electrons and atom nuclei in a partially shielded Coulomb field. The consequence of elastic interaction between beam electrons and electron shells of atoms involves the formation of: diffraction contrast on parallel beam images (TEM), electron diffraction; scanning transmission dark-field images (TSEM), including atomic resolution images, using a Z-contrast technique [2].

Since elastic scattering of an incident electron on a nucleus changes the electron direction, a part of the incident electron energy is always transferred to the nucleus during this process. The energy T transferred to the nucleus depends on the electron scattering angle in the center-of-mass system θ:

$$T = T_{\max} \sin^2(\theta/2), \quad (1)$$

and on the maximum transferred energy $T_{\max}$, which can be transferred by the electron to the nucleus. $T_{\max}$ mainly depends on the nucleus mass and also on the electron energy E_{kin} taking into account the relativistic corrections:

$$T_{\max} = \frac{2E_{kin}}{mc^2}(E_{kin} + 2m_e c^2), \quad (2)$$

where m is the nucleus mass, m_e is the electron rest mass [1].

From (1) it follows that the maximum energy is transferred to the nucleus with „back" scattering of the incident electron, i.e. at $\theta = \pi$. Evaluation of $T_{\max}$ using relation (2) shows that for light nuclei it may be from ten to tens of electron volts, which may be higher than the threshold energy of atomic displacement from the lattice site E_d for atoms within the material as well as especially for atoms in a near-surface region, which may be a significant fraction of all atoms in the irradiated material volume due to a low sample thickness typical of transmission scanning methods. When $T > E_d$ is satisfied, the atom is knocked out of the lattice site and a Frenkel pair is formed.

In terms of electron microscopy, negative consequences of such defect formation in certain conditions may include: electrostatic charging of the sample surface, lattice

disturbance and electron-induced atom scattering from the sample surface [1,3]. However, as will be shown below, controlled directed displacement of light atoms along the initial electron motion path allows target modification of light atom concentration in the irradiated volume, which is accompanied by modification of physical properties and offers the opportunity for forming composite structures for various applications.

Inelastic scattering of beam electrons is the Coulomb interaction between incident electrons and electrons surrounding the atom nuclei in the test sample, and also inelastic scattering during interaction with the nucleus induces braking radiation. Inelastic scattering accompanied by knocking out of the atomic electron results in the following processes: characteristic X-ray quantum (the basis of elemental EDS analysis); incident electron energy loss (the basis of EELS chemical analysis); other processes — secondary electron emission, photo-emission, etc. But inelastic scattering may also lead to formation of atomic damage in the form of a radiolysis process that is mainly typical of dielectrics, ionic crystals, etc., for example, radiolysis results in breaking polymer or halide bonds. The sample may be heated through phonon excitation that is the main source of polymer and biological tissue damage; electronic excitation also induces surface contamination by hydrocarbons (actively diffuse along the surface into the irradiation zone) that shadows and distorts a TEM image [4,5].

Study of radiation damage in various materials, including metal oxides with various oxidation levels, under the action of electron irradiation with electron energy higher than 100 keV is described in detail in review [6]. It was found that radiation damage of metal oxides depended on a set of properties such as microscope's accelerating voltage, current density, beam size, crystal-lattice orientation of the sample, TEM sample preparation technique, and test sample thickness. The review describes theoretical calculations and supporting experimental data to explain the nature of radiation damage phenomena induced in metal oxides in terms of a so-called mechanism of damage by induced electric field (DIEF). This is an approach where an electric field is induced in the sample by positive charges resulting from excitation and ionization during irradiation by high-energy electrons.

Excited atom state relaxation time after knocking out the internal electron is the key parameter for potential implementation of the DIEF mechanism. If this time is long, then considerable Coulomb forces resulting from formation of the charged atom have enough time to displace it from the equilibrium position in the lattice to form a point defect. The relaxation time depends qualitatively on the material's electrical conductivity. For example, for good conductors, relaxation is so quick that the DIEF mechanism is not implemented for them.

In [7], rutile systems, TiO_2 and NiO, are used to compare radiation damage mechanisms in terms of their behavior on the surface and within the material. It was found that TiO_2 is associated with surface ionization damage in the form of desorption induced by electronic transitions (DIET) regardless of the incident electron energy. For NiO, such mechanism is not observed, on the contrary, NiO oxidizes to Ni_3O_4 interacting with oxygen from vacuum in the electron microscope column.

Dose rate dependence and threshold nature of metal oxide reduction induced by electron irradiation were discussed in [8]. It is also shown that this process is reversible for highly reactive metals. CeO_2 was used to show that, when the threshold dose rate is exceeded, oxygen vacancies are formed, which is followed by a change in the oxidation level of Ce ions. Oxygen in residual vapor in the microscope vacuum column oxidizes the sample and restores the damage induced by electron irradiation making this process reversible. Thus, damages are accumulated only when the restoration rate is lower than the material damage rate [8–10].

The effect of high-energy electron irradiation (150 keV) in the TEM column on the structure and chemical composition of alkaline earth metal fluorides, CaF_2, SrF_2 and BaF_2, was studied in [11]. Metal fluorides were found to be very sensitive to electron irradiation that knocks out fluorine atoms from the lattice sites. The authors believe that electron excitations generated by incident beam electrons are the main radiation defect formation mechanism.

Direct knocking out of atoms from the lattice sites due to elastic scattering of beam electrons on nuclei with transfer of the energy T higher than the threshold energy of atom displacement from the lattice site E_d in the beam electron motion direction is considered in this work as the main radiation damage formation mechanism. The incentive behind the consideration of this mechanism is in the fact that it offers the opportunity to remove light atoms from a substance in a controlled manner and, thus, to transform the composition and properties of an irradiated material in a targeted manner. Probability of such interaction between electrons and substance atoms is defined by scattering cross-sections for this process. Other mechanisms associated with electron excitations are not covered in this work because substances studied in it feature good electric conductivity that provides quick relaxation of excited electron state and local ionization fails to induce atomic displacement due to the charging effect. Probabilities of damage due to the charging effects depending on the excited electron state lifetimes are evaluated in [12] to justify the absence of demand for the charging mechanism for conducting materials.

Full cross-section of relativistic electron scattering on the atom with transferred energies from T to $T_{\max}$ according to McKinley and Feshbach [13] is equal to

$$\sigma(T) = \frac{2.49 \cdot 10^{-25} Z^2}{\beta^4 \gamma^2} \left\{ \frac{T_{\max}}{T} - 1 - \beta^2 \ln\left(\frac{T_{\max}}{T}\right) + \pi\alpha\beta \left[2\left\{ \sqrt{\frac{T_{\max}}{T}} - 1 \right\} - \ln\left(\frac{T_{\max}}{T}\right) \right] \right\}, \quad (3)$$

where

$$\gamma = \frac{E_{kin}}{m_e c^2} + 1; \quad \beta = \sqrt{1 - \frac{1}{\gamma^2}}; \quad \alpha = \frac{z}{137}.$$

To calculate full cross-section of processes with transferred energies higher than the threshold displacement energy — atomic displacement cross-section, the threshold energy of atomic displacement from the lattice site shall be substituted into expression (3):

$$\sigma_d = \sigma(E_d). \tag{4}$$

Expression (4) reflects the probability of atom displacement from its lattice site induced by scattering of relativistic beam electrons on the Coulomb nucleus field and such displacements always occur regardless on whether other displaced atom formation mechanisms (electronic subsystem excitation, etc.) may be implemented.

According to this mechanism, the atom displacement rate is calculated as a product of the full displacement cross-section by the density of electron beam (j): $j\sigma_d$.

The magnitude of cross-section (4) depends on the electron energy, atomic number and threshold displacement energy. For light atoms (C, O, S, etc.), electron energy of 200 keV and typical displacement energies (~ 20 eV), cross-section (4) is from units to tens of barn. Taking into account quite a substantial density of electron beam, a significant damaging dose rate buildup rate is attained during electron irradiation in the electron microscope column within reasonably practicable times. Given $\sigma_d \sim 10$ barn, then for typical $j \sim 10^{20}$ e/(cm^2·s) the defect formation rate is $\sim 10^{-3}$ displacements per atom (dpa) per second, accordingly, an irradiation dose rate of 1 dpa is reached with an irradiation time of ~ 16.6 min. According to the terminology used in the radiation solid-state physics, a mean number of displacements per light atom is hereinafter referred to as the irradiation dose rate.

For radiation-induced transformation of solid body properties caused by the change in material's atomic composition, certain kind of atoms shall be preferentially removed from the amount of atoms. In this process, it is important to provide selective atomic displacement [14,15] (this set of methods for selective modification of materials' atomic composition was developed primarily for ionic irradiation) and also to make sure that these atoms are removed preferably in some preferential direction or from the irradiated volume, otherwise, it is difficult to expect that the material phase composition will change when atoms of only one kind are displaced.

Electron irradiation to a greater degree induces directional atomic displacements because the knock-on atom receives a pulse along the initial electron motion direction due to a big difference in the electron and displaced atom masses. Thus, for example, it was demonstrated in [16] that exposure of a diatomic compound film to 200 keV electron irradiation in the electron microscope column induces phase transition (with intermediate amorphous state of the substance) caused by removal of light atoms from the film material under the action of electron irradiation.

Thus, transmission electron microscopy is simultaneously used to produce such directional atomic displacements during exposure to high-energy electrons and to examine the variation of materials' structure and phase composition.

Thus, *in situ* irradiation of materials in the electron microscope offers wide opportunities for studying both selectivity and directionality of atomic displacements during irradiation. First, by varying the mono-energetic beam energy, the transferred energy may be controlled quite accurately to achieve the defect formation selectivity for various atoms. Second, due to low electron mass and fundamentally low exceedances of the maximum transferred energy over the threshold energy, displacing interactions between electrons and nuclei occur in a narrow scattering angle range, and this means that the primary knocked-on atom (PKA) receives a pulse also in a narrow angle range, i.e. there is directional PKA displacement.

Since PKA receives energy that only slightly exceeds the threshold energy, the most part of energy is spent to bring PKA outside the spontaneous recombination volume. Remaining energy is from unit to tens of electron-volts, which is insufficient for any further significant movements in the lattice. Therefore, it can be believed that PKA moves at a distance equal to the radius of spontaneous recombination sphere in the direction of the received pulse.

Since the free path lengths of the employed electrons are much larger than the sample thickness in the exposed areas, atoms are displaced one-by-one and evenly across the material volume. Long-term irradiation results in reduction of the displaced atom concentration due to gradual movement along the beam followed by going outside the sample on its rear side. Reduction of atom concentration in a solid body initiates both structural and phase transformations. Experimental measurement of phase transition conditions resulting from a change in materials' atomic composition induced by electron irradiation is used to study the directional atomic displacement process.

1. Experimental

1.1. Samples

The following materials are used in this work as survey items.

1.BiO_2 deposited in a 20 nm thin film at room temperature onto rock salt coated with a thin amorphous diamond-like carbon layer. Amorphous carbon and BiO_2 films were deposited stepwise onto a fresh cross-section of the NaCl single crystal by cathode sputtering at room temperature of the substrate [17]. Bismuth oxide consists of heavy metal atoms, for which maximum transferred energy for electrons is low ($T_{\max} \sim 2.5$ eV), and of light oxygen atoms, to which electrons can transfer energies exceeding the threshold displacement energies for oxygen atoms E_d ($T_{\max} \sim 32$ eV).

2. CuO also deposited in a 20 nm thin film onto rock salt coated with a thin amorphous carbon layer by cathode sputtering at room temperature [17].

3. Thin cross-section cut from theTaS_2 crystal using a focused ion beam (FIB) system.

After sputtering, bismuth oxide (1) and copper oxide (2) samples were placed onto standard copper TEM grids after rock salt dissolution.

Irradiation was performed *in situ* in a transmission electron microscope column. The „TEMSCAN-200CX“ (Jeol) electron microscope with a hot cathode made of W and „Titan 80-300ST“ (FEI) electron microscope with a Schottky cathode. Irradiation was carried out at room temperature. Electron energy was 200 keV.

Electron current density (j) was determined as a ratio of current (I) to the smallest apparent beam area in TEM mode ($S_{\min}$): $j = I/S_{\min}$.

Beam current was measured in the „TEMSCAN-200CX“ using the Faraday cylinder and in the „Titan 80-300ST“ using readings of the embedded electron current sensor through a fluorescent screen. The obtained electron beam current density measured by the „TEMSCAN-200CX“ was $0.81 \cdot 10^{20}$ e/(cm^2·s) and by the „Titan 80-300ST“ was $2.9 \cdot 10^{20}$ e/(cm^2·s).

Since the *in situ* irradiation experiments using an electron microscope take a long time, it is important to control the irradiation region identity compensating the sample drift effect. For this, some typical reference point, for example, a film defect, etc., is chosen on the TEM image of the irradiated sample area. At the beginning of experiment, the irradiated area was positioned with respect to the reference point position and held in this position throughout the irradiation experiment by visual inspection on the fluorescent microscope screen with the required manual drift correction using horizontal movement adjustment of the sample holder. The irradiation experiment used the minimum TEM beam size.

Condition of the irradiated sample area was recorded both by the microdiffraction pattern and Fourier transform patterns from electron microscopy images with high resolution, as well as by means of the analysis of energy loss spectra of electrons transmitted through the sample.

Electron energy loss spectroscopy was performed using the „Titan 80-300ST“ transmission electron microscope without spherical aberration corrector, equipped with the Gatan „GIF-2001“ parallel-detection electron energy loss spectrometer. Electron energy loss spectra were recorded in the STEM mode (microscope was set to diffraction mode). The following settings were used for effective spectra recording: electron beam convergence angle $\alpha = 10$ mrad with a probe size of $d_t = 0.14$ nm, spectrometer input aperture 3 mm, camera length 60 mm, spectrometer lead angle β was 14.82 mrad. Quantitative analysis used a standard film-depth relative concentration method.

2. Findings and discussion

Electron microscopic investigations showed that the irradiation process involved a number of successive solid-state phase transformations of the original BiO_2 first into Bi_2O_3 and then into metallic bismuth (Bi) during more long-term irradiation.

Figure 1 shows electron-microscopy photographs of the irradiated area microstructure with visible original oxide regions A and region B where oxide with reduced oxygen concentration, Bi_2O_3, was formed by irradiation to $1.5 \cdot 10^{23}$ e/cm^2. According to Figure 1, a, Bi_2O_3 features

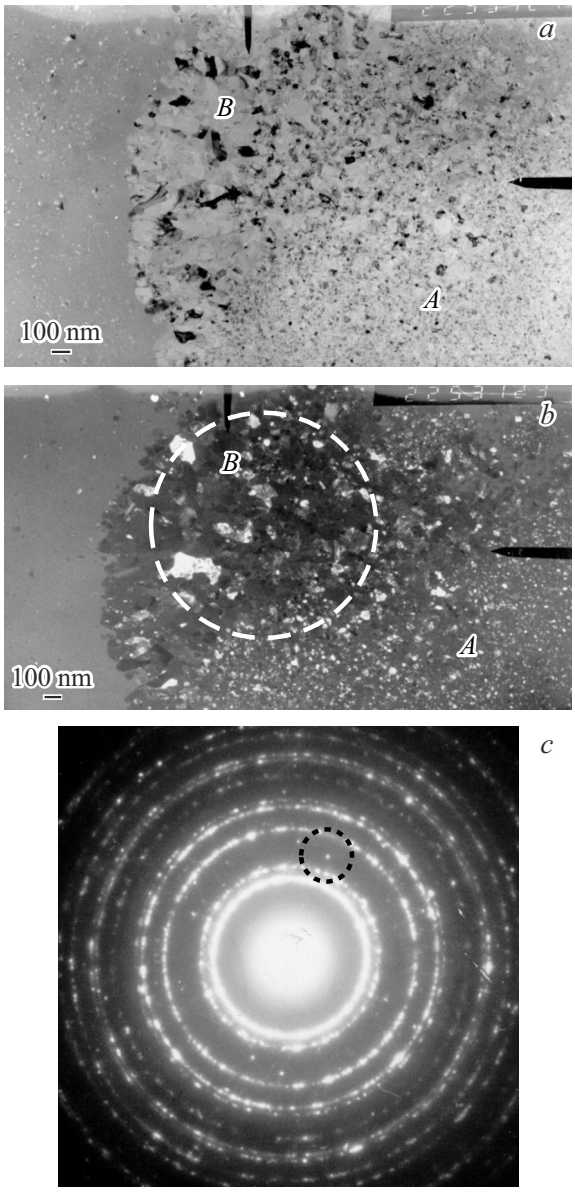

Figure 1. Electron microscopy images of unirradiated BiO_2 region (A) and Bi_2O_3 region irradiated to an electron fluence of $1.5 \cdot 10^{23}$ e/cm^2 (B): a — bright field; b — dark field; c — microdiffraction pattern of electrons from the modified Bi_2O_3 for an electron fluence of $1.5 \cdot 10^{23}$ e/cm^2 (aperture diaphragm position during dark-field imaging is shown with dashed line (b)).

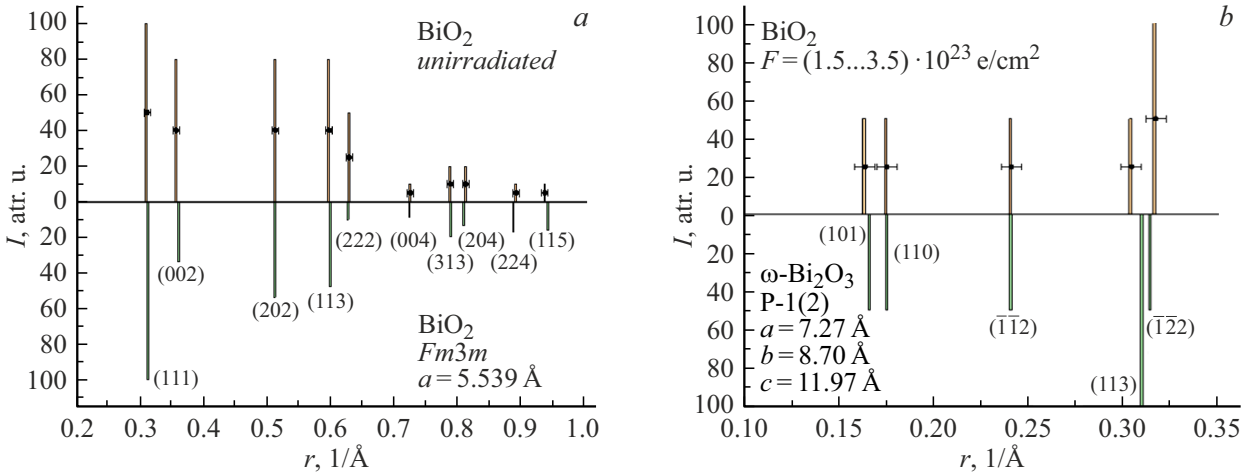

Figure 2. Diagrams of lines on the electron microdiffraction patterns: *a* — of the original bismuth oxide (top) and of BiO_2 (bottom); *b* — of the modified bismuth oxide (electron fluence $(1.5-3.5) \cdot 10^{23}$ e/cm^2) (top) and of Bi_2O_3 (bottom).

a larger grain size. Figure 1, *b* shows dark-field electron microscopy image recorded with the aperture diaphragm set in the area of new emerging reflections between the second and third polycrystalline lines of the original BiO_2 (Figure 1, *c*, aperture diaphragm position is shown with a dashed line) with a clearly visible increase in the grain size in the modified oxide by ten times and more. Note that, since the crystal reflections of the modified and original oxide are close to each other on the electron diffraction pattern, the reflections cannot be fully separated due to a fixed aperture diaphragm size, therefore some BiO_2 grains can be seen in the dark field together with Bi_2O_3 grains. Large grain size of the modified Bi_2O_3 shows up on the electron diffraction pattern in the form of single reflections from grains of the formed phase between the polycrystalline lines of the originalBiO_2.

Microstructure modifications that are visible by the microscope and caused by irradiation-induced phase transformations as illustrated in Figure 1 were experimentally supported by precision analysis of diffraction ring diameters on the electron diffraction patterns (Figure 2) made on photographic film using an optical comparator to provide a straight-line distance measurement accuracy of ~ 0.01 mm with a typical first diffraction ring diameter of ~ 8.68 mm. Therefore, all results concerning the phase transformation behavior obtained in this work are based on the review of electron diffraction patterns or Fourier transform patterns from direct atomic-resolution images.

Figure 2, *a* at the top shows a diagram of polycrystalline line position measurements (a distance from the center of electron diffraction pattern is plotted on the x axis) of the original bismuth oxide, and Figure 2, *a* at the bottom shows the literature data [18] concerning the polycrystalline diffraction line layout for BiO_2 with a cubic crystal system (Fm3m) and $a = 5.539$ Å with specified line indices. According to these measurements, a conclusion is made that the original phase in our experiments corresponds to BiO_2 with a cubic crystal system.

Figure 2, *b* at the top shows a diagram of polycrystalline line position measurements for BiO_2 irradiated to $3.5 \cdot 10^{23}$ e/cm^2 in the reciprocal space region with distances to center shorter than the radius of the first ring for the original BiO_2, and Figure 2, *b* at the bottom shows the literature data [19] concerning the polycrystalline diffraction line layout for Bi_2O_3 with the triclinic crystal system P-1(2) and $a = 7.270$ Å, $b = 8.694$ Å, $c = 11.97$ Å, $\alpha = 87.713°$, $\beta = 93.227°$, $\gamma = 86.653°$, specifying the line indices. According to these measurements, a conclusion is made that the irradiation-induced bismuth oxide phase corresponds to Bi_2O_3 with a triclinic crystal system.

The summary for electron irradiation of BiO_2 is given below:

- when the electron fluence is $1.5 \cdot 10^{23}$ e/cm^2, electron diffraction patterns show the first signs (reflections) of intermediate Bi_2O_3 with lower oxygen concentration (60 at.%) compared with the original one (66 at.%). The electron fluence (F) was calculated by multiplying the irradiation time by the density of electron beam: $F = j \cdot t$;
- further electron irradiation in the dose rate range of $(1.5-3.5) \cdot 10^{23}$ e/cm^2 initiates further removal of oxygen atoms from the sample followed by the enhancement of diffraction reflections from the modified Bi_2O_3 indicating that the Bi_2O_3 formation process propagates deeply into the sample.

Irradiation of original copper oxide thin film goes in the same way. According to microdiffraction pattern interpretation data (Figure 3, *a*), the copper oxide was identified as polycrystalline CuO with a monoclinic crystal system and $a = 4.685$ Å, $b = 3.426$ Å, $c = 5.130$ Å, $\beta = 99.55°$ [20]. Figure 3, *a* at the top shows positions of diffraction lines from the original sample, at the bottom — shows the literature data concerning the line positions in CuO [20].

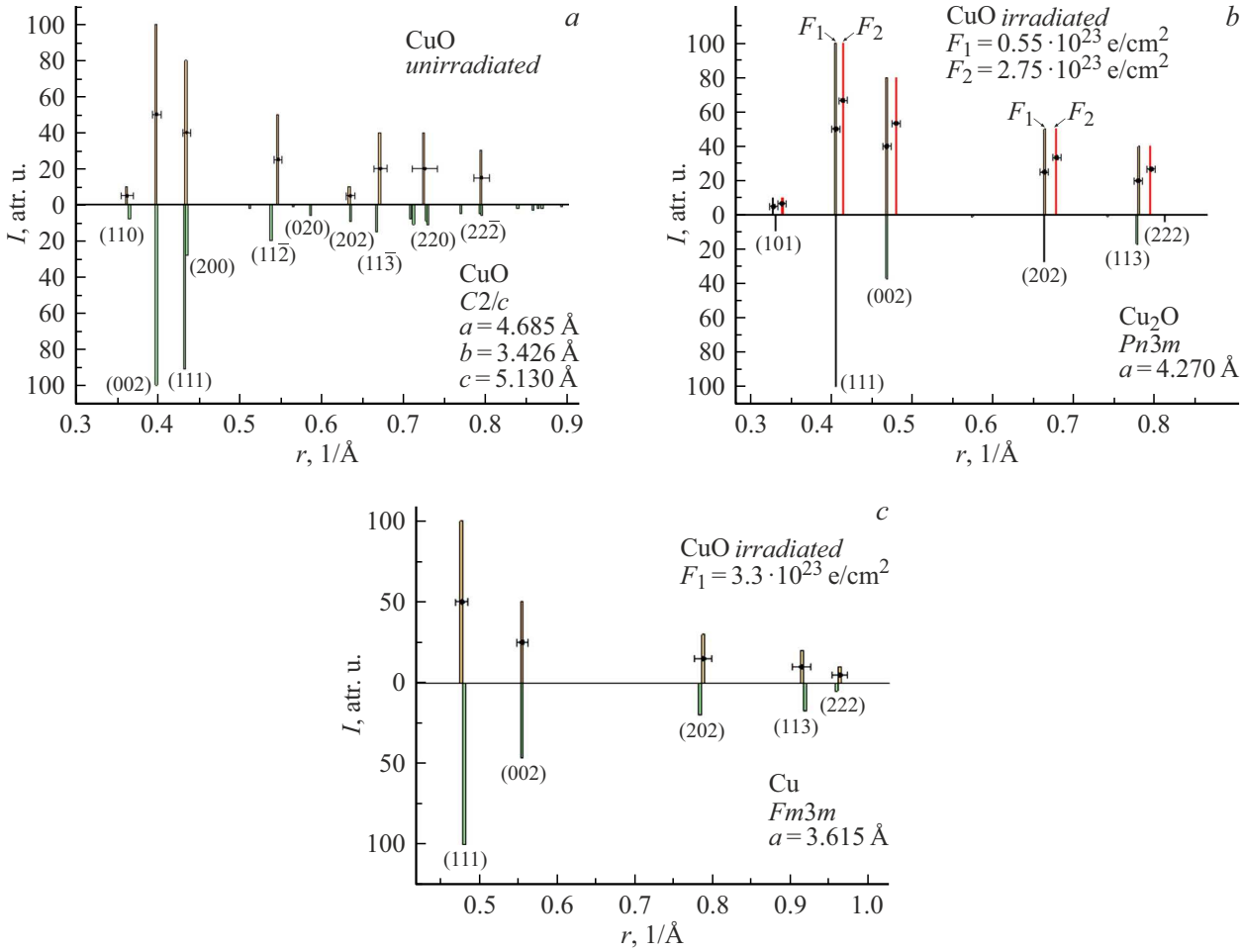

Figure 3. Diagrams of lines on the electron microdiffraction patterns: *a* — of the original copper oxide (top) and CuO (bottom); *b* — of the modified copper oxide after irradiation to $F_1 = 0.55 \cdot 10^{23}$ e/cm^2 and to $F_2 = 2.75 \cdot 10^{23}$ e/cm^2 (top) and of Cu_2O (bottom); *c* — of oxide irradiated to$3.3 \cdot 10^{23}$ e/cm^2 (top) and of metallic copper (bottom).

After irradiation by electrons to $F_1 = 0.55 \cdot 10^{23}$ e/cm^2, the electron diffraction pattern changes and corresponds to Cu_2O. This follows from comparison of the diffraction line layout on the electron diffraction pattern of the irradiated sample and of the literature data concerning the layout of lines from Cu_2O with the cubic crystal system Pn3m and $a = 4.27$ Å (Figure 3, *b*) [21].

Further irradiation to $F_2 = 2.75 \cdot 10^{23}$ e/cm^2 causes a decrease in the lattice parameter of Cu_2O (by an increase in the diffraction line radius) due to removal of oxygen atoms from the modified oxide with maintaining theCu_2O phase — this is shown by line displacement into a larger radii region (lines for F_2 in Figure 3, *b*).

Increase in the fluence up to $3.3 \cdot 10^{23}$ e/cm^2 leads to formation of metallic copper, which is demonstrated by the experimental diffraction lines (Figure 3, *c* top half) corresponding to the lines of metallic copper with the cubic crystal system Fm3m and $a = 3.615$ Å (Figure 3, *c* bottom half) [22].

The summary for electron irradiation of CuO is given below:

- the electron fluence of $0.55 \cdot 10^{23}$ e/cm^2 induces intermediate Cu_2O with a lower oxygen concentration (33 at.%) compared with the original level (50 at.%);
- further electron irradiation in the fluence range of $(0.55-2.75) \cdot 10^{23}$ e/cm^2 initiates oxygen atom removal followed by a decrease in the Cu_2O lattice parameter;
- achievement of $3.3 \cdot 10^{23}$ e/cm^2 initiates formation of metallic copper (Cu).

Electron irradiation of polycrystalline TaS_2 also results in removal of a light sulfur atom from the crystal due to gradual displacements along the electron beam direction. Figure 4, *a* shows TEM images of the original tantalum sulfide grains and the Fourier transform pattern, by which they were identified as the TaS_2 phase with the hexagonal crystal system P3m1 and $a = 3.385$ Å, $c = 5.9$ Å [23].

After electron irradiation to $\sim 1.74 \cdot 10^{23}$ e/cm^2, phase transition of the original TaS_2 (atomic concentration of S is 66 at.%) (Figure 4, *a*) takes place to form tantalum sulfide with low S content, TaS, (atomic concentration of S is 50 at.%) (Figure 4, *b*) with the hexagonal crystal system P6m2 and $a = 3.27$ Å, $c = 3.125$ Å. Formation of

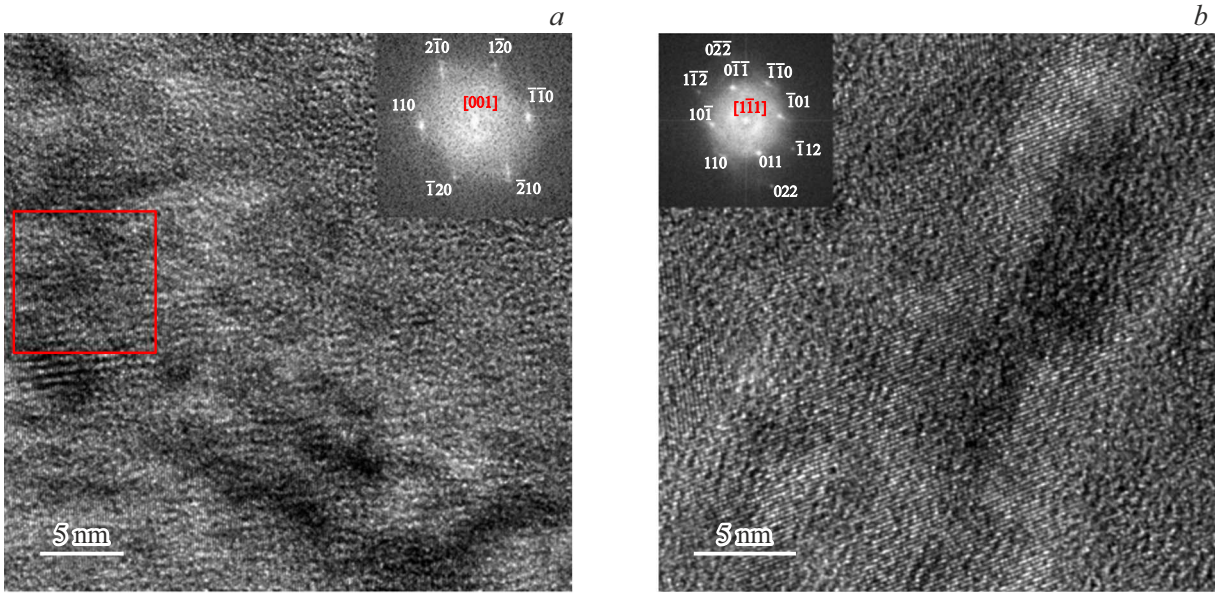

Figure 4. *a* — TEM image of the original TaS_2, inset — Fourier transform pattern from the TaS_2 image; *b* — TEM image of TaS formed after irradiation to $1.74 \cdot 10^{23}$ e/cm^2, inset — Fourier transform pattern from the TaS image.

a new TaS phase is also supported by processing of data obtained from the electron energy loss spectra (Figure 5, *a*) of the original *1* and irradiated *2* regions of the material. Figure 5, *b, c* shows the electron energy loss spectra processing data for determining the atomic concentrations of Ta and S for a series of points.

2.1. Model of atom removal process induced by electron irradiation

Suppose that with each displacement the displaced light atom effectively moves at some distance L along the electron beam direction. Assume that this mean distance doesn't depend on the magnitude of energy transferred to PKA (Primary Knock-on atom) and on the local composition of the target material. The first assumption may be considered to be perfectly acceptable because when the maximum transferred energy is a little higher than the threshold displacement energy E_d, PKA energy remaining after removal outside the spontaneous recombination region (several electron-volts) cannot lead to significant PKA movements in the lattice. The second assumption probably also quite accurately describes the situation in this case because the general irradiation-induced modification of atomic composition is not high at least at the initial stage.

With uniform atomic displacement across the sample volume, the concentration of light atoms starts decreasing from the surface, on which the electron beam falls. This is because any other element deep in the sample or near the rear surface receives the same amount of atoms per unit time from a volume spaced from the element at the distance L closer to the front surface of the sample as the element looses due to irradiation-induced atomic displacements.

Change in the concentration $n(x, t)$ of the displaced atoms at the distance x from the surface per the time period dt is equal to:

$$dn(x, t) = j\sigma_d n(x - L, t)dt - j\sigma_d n(x, t)dt, \qquad (5)$$

where the second term describes the atom concentration loss due to displacements in the layer with the x-coordinate, and the first term describes the corresponding increase in the concentration due to displacements in the layer with the $x-L$-coordinate.

We separate the sample into layers with the thickness L parallel to the surface. Then for a layer closest to the surface, referred to as the zero layer, the first term of the difference in expression (5) will be equal to zero because atoms displaced from the previous layer don't get into this layer. Equation (5) becomes homogeneous and have a simple exponential solution:

$$n_0(t) = N_0 e^{-j\sigma_d t} = N_0 e^{-\lambda t}, \qquad (6)$$

where the defect generation rate is denoted as $\lambda = j\sigma_d$, the subscript of $n(t)$ denotes a layer number, and N_0 is the initial concentration of light atoms in the sample.

For the next (first) layer, the minuend in expression (5) is nonzero, and $n(x-L, t)$ corresponds to the atom concentration in the zero layer (6). Equation for concentration in the first layer becomes inhomogeneous:

$$\frac{dn_1(t)}{dt} + \lambda n_1(t) = \lambda N_0 e^{-\lambda t}. \qquad (7)$$

Bernoulli equation (7) has the following solution

$$n_1(t) = N_0 e^{-\lambda t}(\lambda t + 1). \qquad (8)$$

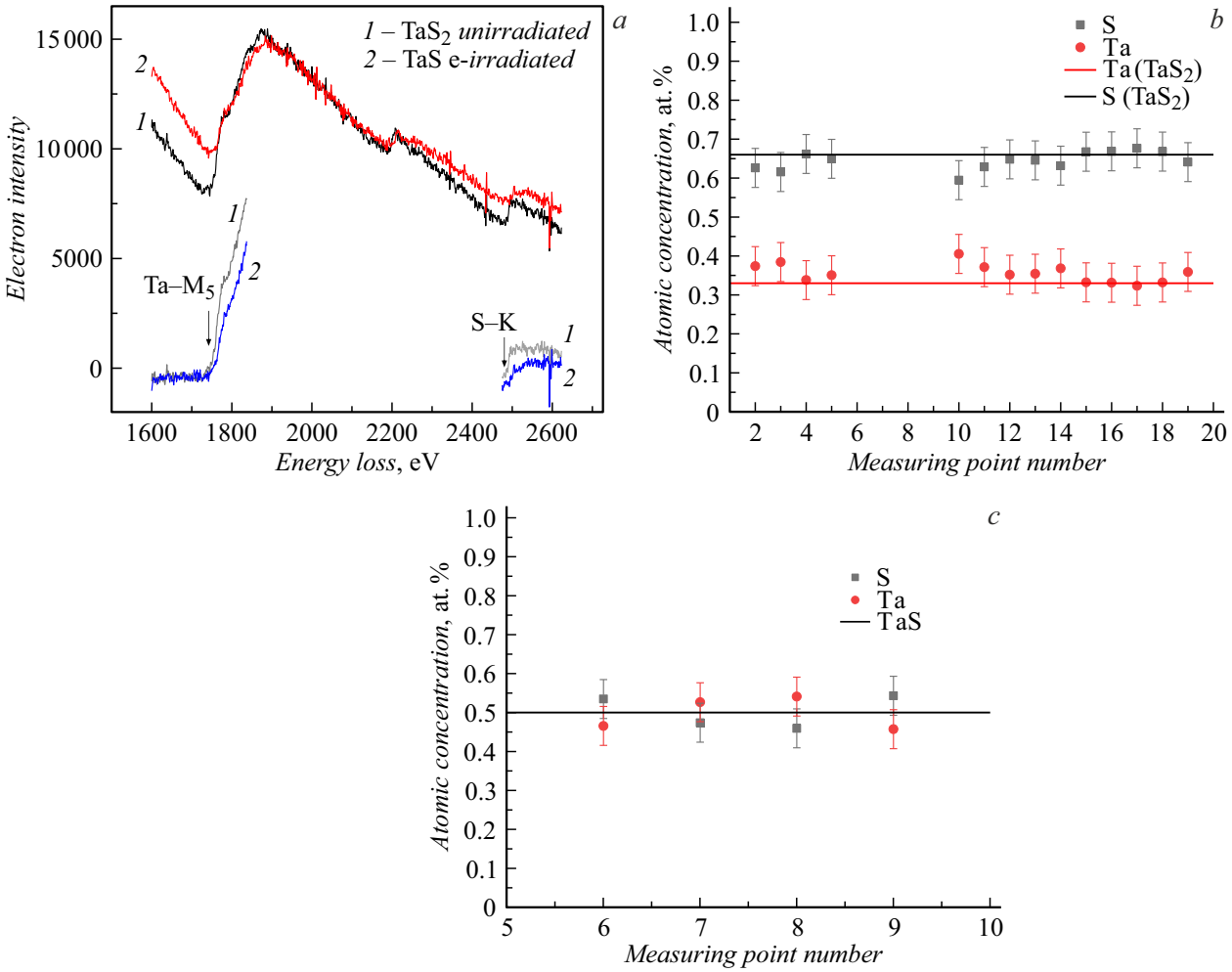

Figure 5. EELS lines of Ta and S used for the elemental analysis. *a* — *1* — for the original sample (TaS_2), *2* — after irradiation to $1.74 \cdot 10^{23}$ e/cm^2 (TaS). Atomic concentrations of elements in the original (*b*) TaS_2 and after irradiation (*c*) to $1.74 \cdot 10^{23}$ e/cm^2 in the formed TaS for a series of measured points.

For the second layer, the differential equation of dependence of $n_2(t)$ on time will be written similar to (7), but only function (8) will occur after λ on the right-hand side because the increase in oxygen atoms in the second layer is caused by atomic displacement from the first layer.

It is apparent that generally for layer i the dependence of $n_i(t)$ on time will be written as

$$n_i(t) = N_0 e^{-\lambda t}\left(\frac{(\lambda t)^i}{i!} + \ldots + 1\right). \qquad (9)$$

Figure 6 shows the calculated curves (9) demonstrating the change in oxygen atom concentration on various layers depending on the irradiation dose rate expressed in dpa.

Figure 6 may be used to compare the calculated and experimental data obtained in this work and to evaluate the parameters of light atom removal from lattice sites of the original material resulting from directional atomic displacement by beam electrons.

For correct comparison of the experimental and calculated data, we derive a simple relation between the number

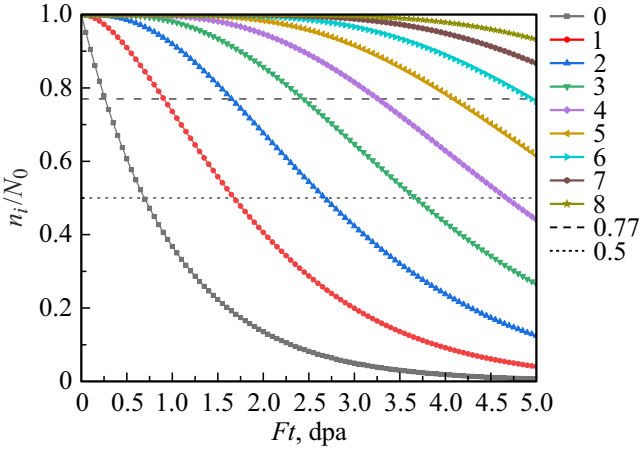

Figure 6. Model light element concentration reduction curves.

of remaining light atoms in the irradiated material and the initial number of light atoms in the original material on

the assumption that the irradiation-induced variation of the number of other (heavy) atoms may be neglected.

Let the light atom concentration in the original substance is c_1, in the irradiated substance is c_2, and the initial number of all atoms in the original substance is N. Let the number of light atoms decreases by ΔN under irradiation. Then an equation may be written to relate the number of light atoms in the irradiated material to the initial number of light atoms including the atom loss:

$$c_2(N - \Delta N) = c_1 N - \Delta N. \quad (10)$$

By a little manipulation, from relation (10) we get the relation of the number of light atoms in the irradiated material (N) to the number of light atoms in the initial material (N_0):

$$\frac{N}{N_0} = \frac{c_2(1 - c_1)}{c_1(1 - c_2)}. \quad (11)$$

2.2. Procedure for comparing the experimental and calculated data to evaluate the physical parameters of interaction between electrons and target atoms

The main experimentally recorded parameters of solid-state transformations include the electron irradiation fluence (F_1), at which the signs of early formation of new phases with lower concentration of light atoms occur and are identified using the electron diffraction patterns, Fourier transform patterns from direct atomic-resolution images, dark-field and bright-field TEM images,electron energy loss spectra, etc.

However, it should be born in mind that a decrease in concentration of light atoms during directional displacements induced by electron irradiation starts from the sample surface (zero layer in Figure 6) facing the electron source, and in deeper layers, this transformation will take place at a higher fluence than in the zero layer because atoms removed from them are replaced by new atoms from overlying layers. Therefore, when the signs of early formation of new phases are observed, for example, new lines, reflections on the electron diffraction pattern, there is also a diffraction pattern from the original phase on these electron diffraction patterns. For the diffraction pattern from the original substance to fully disappear, much higher electron irradiation fluence is usually required. In some cases, full removal of light atoms can be achieved (reduction to metallic state), which is characterized by the second fluence value (F_2), but it should be also considered that full reduction primarily occurs in the zero layer (Figure 6). Therefore, when comparing the experimental fluence data and calculated data in Figure 6, the main focus is made on the zero layer.

When an experimental value of F_1 and relation of the number of light atoms to the initial number of atoms (N/N_0) typical for this transformation are known (see (11)), then curve „0“ in Figure 6 is used to find the corresponding irradiation dose rate expressed in displacements per atom $(Ft)_1$ (dpa). This point shows how many displacements per light atom must be reached in the zero layer to get the number of light atoms in it decreased to the required criterion. Then, by dividing the obtained $(Ft)_1$ by F_1 expressed in e/cm^2, we get an estimated cross-section

$$\sigma_d = \frac{(Ft)_1}{F_1}. \quad (12)$$

Then, from the obtained cross-section (12), the threshold energy of atomic displacement from the lattice site is calculated using equation (4) E_d.

2.3. Bismuth oxide electron irradiation

According to the review of electron microdiffraction patterns (Figure 2, *a*), the state of original film corresponded to BiO_2. After irradiation to $F_1 = 1.5 \cdot 10^{23}$ e/cm^2, reflections from the modified Bi_2O_3 are observed. A decrease in the number of oxygen atoms with respect to the number of oxygen atoms (see relation (11)) in the original (BiO_2) $n_i/N_0 = 0.77$ corresponds to Bi_2O_3. This value is shown with the upper dashed line in Figure 6 that intersects the curve for the zero layer at 0.264 dpa Using equation (12), taking into account F_1, a cross-section of 1.76 b is obtained, consequently, the threshold oxygen atom displacement energy is 31.3 eV.

2.4. Copper oxide electron irradiation

The same removal of oxygen atoms from copper oxide induced by 200 keV electron irradiation was demonstrated during irradiation of a thin film sample in the electron microscope column. Review of the electron microdiffraction patterns (Figure 3, *a*) shows that the state of original film corresponded to CuO. After irradiation to $F_1 = 0.55 \cdot 10^{23}$ e/cm^2, CuO is transformed to Cu_2O with lower oxygen concentration compared with the original oxide. Formation of Cu_2O from CuO using equation (11) is followed by a decrease in oxygen atom concentration to $n_i/N_0 = 0.5$, which, for the zero layer in Figure 6, occurs at ~ 0.7 dpa (middle dashed line in Figure 6). Using equation (12), including F_1, we get a cross-section of ~ 12.73 b, consequently, the threshold displacement energy is 21.5 eV.

As the irradiation fluence increases to $F_2 = 2.9 \cdot 10^{23}$ e/cm^2, the Cu_2O lattice parameter decreases indicating that knocked-on oxygen atoms are removed from the film material. Further irradiation induces formation of reduced copper at $\sim 3.3 \cdot 10^{23}$ e/cm^2 (Figure 3, *c*). With the obtained cross-section of ~ 12.73 b, the experimental fluence of $\sim 3.3 \cdot 10^{23}$ e/cm^2 corresponds to the damage level of 4.2 dpa.

2.5. Tantalum sulfide electron irradiation

After irradiation of original TaS_2 to $F_1 = 1.74 \cdot 10^{23}$ e/cm^2, TaS is transformed into TaS

Obtained cross-sections and threshold light atom displacement energies under 200 keV electron irradiation

Substance	Displaced atom	σ_d, b	E_d, eV
BiO_2	O	1.76	31.3
CuO	O	12.73	21.5
TaS_2	S	4.02	15.2

with lower sulfur concentration. Formation of TaS from TaS_2 using equation (11) is followed by a decrease in oxygen atom concentration to $n_i/N_0 = 0.5$, which, for the zero layer in Figure 6, occurs at ~ 0.7 dpa (middle dashed line in Figure 6). Using equation (12) taking into account F_1, we get ~ 4.02 b, which corresponds to the threshold energy of sulfur atom displacement from the lattice sites of 15.2 eV. Such threshold energy corresponds to data obtained in earlier studies of neutron irradiation TaS_2 [24,25].

Generalized results obtained in this work by comparing the experimental electron irradiation fluences (at which phase transformations are observed) with the calculated fluences within the developed model are shown in the table.

Conclusion

The work shows that solid-state transitions are possible in BiO_2, CuO and TaS_2 with formation of phases with lower concentration of light atoms resulting from directional displacements of light atoms interacting with 200 keV electrons. A model is proposed for describing a change in light atom concentration over the sample depth during electron irradiation. A method is proposed for determining the threshold energies of light atom displacement from the lattice sites by comparing the experimental and calculated fluences within the developed model. Analysis of the obtained data allowed quantitative comparison of the proposed model representations concerning the oxygen atom removal mechanisms with the experimental data and provided displacement cross-sections and threshold oxygen and sulfur atom displacement energies in the studied compounds during interaction with electrons.

The findings may be used to develop a technique of directional modification of thin-film material properties by a focused electron probe to create functional elements with desired properties in the required places on the wafer surface. It is also possible to form hybrid devices where „service“ electronics is formed in lower „layers“, for example, using a standard VLSI technology, and the upper „functional“ layer contains a set of service functional elements made using electron-beam probe methods, for example, nanoscale sensors, etc.

Funding

This study was carried out under the state assignment of the National Research Center „Kurchatov Institute.“

Conflict of interest

The authors declare no conflict of interest.

References

[1] R.F. Egerton, P. Li, M. Malac. Micron, **35** (6), 399 (2004). DOI: 10.1016/j.micron.2004.02.003
[2] D.B. Williams, C.B. Carter. *Transmission Electron Microscopy: A Textbook for Materials Science* (Springer, NY., 2009)
[3] R.F. Egerton. Ultramicroscopy, **127**, 100 (2013). DOI: 10.1016/j.ultramic.2012.07.006
[4] R.F. Egerton. Microsc. Res. Tech., **75** (11), 1550 (2012). DOI: 10.1002/jemt.22099
[5] R.F. Egerton. Micron., **119**, 72 (2019). DOI: 10.1016/j.micron.2019.01.005
[6] N. Jiang. Reports Prog. Phys. IOP Publishing, **79**, 016501 (2016). DOI: 10.1088/0034-4885/79/1/016501
[7] M.I. Buckett, J. Strane, D.E. Luzzi, J.P. Zhang, B.W. Wessels, L.D. Marks. Ultramicroscopy, **29**, 217 (1989).
[8] L.A.J. Garvie, P.R. Buseck. J. Phys. Chem. Solids, **60** (12), 1943 (1999). DOI: 10.1016/S0022-3697(99)00218-8
[9] S.R. Gilliss, J. Bentley, C.B. Carter. Appl. Surf. Sci., **241** (1–2), 61 (2005). DOI: 10.1016/j.apsusc.2004.09.018
[10] A.C. Johnston-Peck, J.S. DuChene, A.D. Roberts, D. Wei, A.A. Herzing. Ultramicroscopy, **170**, 1 (2016). DOI: 10.1016/j.ultramic.2016.07.002
[11] V.I.Nikolaichuk, B.P.Sobolev, M.A.Zaporozhets, A.S.Avilov. Kristallografiya, **57** (2), 348 (2012) (in Russian).
[12] D.Sindro, T Oikava. *Analiticheskaya prosvetchivayushchaya elektronnaya mikroskopiya* (Mir, M., 2006) (in Russian)
[13] W.A. McKinley, H. Feshbach. Phys. Rev., **74**, 1759 (1948). DOI: 10.1103/PhysRev.74.1759
[14] B.A. Gurovich, K.E. Prikhod'ko. Phys. Usp., **52**, 165 (2009). DOI: 10.3367/UFNe.0179.200902d.0179
[15] B.A. Gurovich, K.E. Prikhod'ko, E.A. Kuleshova, K.I. Maslakov, D.A. Komarov. J. Exp. Theor. Phys., **116**, 916 (2013). DOI: 10.1134/S1063776113050191
[16] B.A. Gurovich, D.I. Dolgii, E.A. Kuleshova, E.P. Velikhov, E.D. Ol'shanskii, A.G. Domantovskii, B.A. Aronzon, E.Z. Meilikhov. Phys. Usp., **44**, 95 (2001). DOI: 10.1070/PU2001v044n01ABEH000868
[17] D.I. Dolgii, E.D. Ol'shanskii, E.P. Ryazantsev. Konversiya v mashinostroenii, **3–4**, 119, (1999) (in Russian).
[18] B. Begemann, M. Jansen. J. Less-Common Met., **156** (1–2), 123 (1989). DOI: https://doi.org/10.1016/0022-5088(89)90412-8
[19] A.F. Gualtieri, S. Immovilli, M. Prudenziati. Powder Diffr., **12** (2), 90 (1997). DOI: 10.1017/S0885715600009490
[20] N.E. Brese, M. O'Keeffe, B.L. Ramakrishna, R.B. Von Dreele. J. Solid State Chem., **89** (1), 184 (1990). DOI: 10.1016/0022-4596(90)90310-T
[21] R. Restori, D. Schwarzenbach. Acta Crystallogr. B, **42**, 201 (1986). DOI: 10.1107/S0108768186098336
[22] H.E. Swanson, M.C. Morris, E.H. Evans, L. Ulmer. *Standard X-ray Diffraction Powder Patterns* (National Bureau of Standarts, Washington DC, 1964)
[23] W. Blitz, A. Kocher. Z. Anorg. Allg. Chem., **85**, 237 (1938).
[24] H. Mutka, D. Lesueur, L. Zuppiroli. Radiat. Eff., **45** (3–4), 219 (1980). DOI: 10.1080/00337578008208433
[25] D. Lesueur, J. Morillo, H. Mutkaj, A. Audouard, J.C. Jousset. Radiat. Eff., **77** (1–2), 125 (1983). DOI: 10.1080/00337578308224729

Translated by E.Ilinskaya